Molecular BioSystems

Dynamic Article Links

Cite this: *Mol. BioSyst.*, 2011, **7**, 2622–2636

www.rsc.org/molecularbiosystems

**PAPER**

# Modeling synergistic drug inhibition of *Mycobacterium tuberculosis* growth in murine macrophages†

**Xin Fang, Anders Wallqvist and Jaques Reifman***

***Received 15th March 2011, Accepted 31st May 2011***
**DOI: 10.1039/c1mb05106g**

We developed a metabolism-based systems biology framework to model drug-induced growth inhibition of *Mycobacterium tuberculosis* in murine macrophage cells. We used it to simulate *ex vivo* bacterial growth inhibition due to 3-nitropropionate (3-NP) and calculated the corresponding time- and drug concentration-dependent dose-response curves. 3-NP targets the isocitrate lyase 1 (ICL1) and ICL2 enzymes in the glyoxylate shunt, an essential component in carbon metabolism of many important prokaryotic organisms. We used the framework to *in silico* mimic drugging additional enzymes in combination with 3-NP to understand how synergy can arise among metabolic enzyme targets. In particular, we focused on exploring additional targets among the central carbon metabolism pathways and ascertaining the impact of jointly inhibiting these targets and the ICL1/ICL2 enzymes. Thus, additionally inhibiting the malate synthase (MS) enzyme in the glyoxylate shunt did not produce synergistic effects, whereas additional inhibition of the glycerol-3-phosphate dehydrogenase (G3PD) enzyme showed a reduction in bacterial growth beyond what each single inhibition could achieve. Whereas the ICL1/ICL2-MS pair essentially works on the same branch of the metabolic pathway processing lipids as carbon sources (the glyoxylate shunt), the ICL1/ICL2-G3PD pair inhibition targets different branches among the lipid utilization pathways. This allowed the ICL1/ICL2-G3PD drug combination to synergistically inhibit carbon processing and ultimately affect cellular growth. Our previously developed model for *in vitro* conditions failed to capture these effects, highlighting the importance of constructing accurate representations of the experimental *ex vivo* macrophage system.

## Introduction

Tuberculosis (TB) remains a potential health threat to the general United States population, but the main burden of the disease is felt worldwide, with 9.4 million new cases and 1.8 million deaths in 2008.[1,2] The causative agent of the disease, *Mycobacterium tuberculosis*, latently infects one-third of the world's human population.[3] Current efforts to treat and eliminate TB are hindered by the complexity of drug regimens, the appearance of drug-resistant strains of *M. tuberculosis*, and the emergence of a patient population with compromised immune systems.[3,4] Although current therapies include a combination of drugs that inhibits both metabolic and non-metabolic targets, these therapies will inevitably become less effective. The continued reliance on drugs to combat this disease necessitates a continuous search for new druggable targets and combination therapies.[5]

The search for novel bacterial drug targets and drug strategies is aided by recent genome-scale metabolic network reconstructions of several pathogenic organisms,[6–10] including *M. tuberculosis*.[11,12] These reconstructions can be used to understand species-specific differences among bacteria, *e.g.*, mycolic acid utilization for Mycobacteria, the determination of nutrient requirements and metabolite processing steps, and the ability to probe metabolic enzymes/pathways for possible drug targets. Analyzing and probing these systems require systems biology tools to account for hundreds to thousands of metabolites and enzymes. Specifically, metabolic network reconstructions are primarily geared for studying metabolite processing and cell growth phenotypes. For example, given the availability of a specific set of nutrients, flux balance analysis (FBA) of metabolic networks can predict microbial growth rates.[11–15] Metabolic network analysis can also help identify the essential genes of an organism, *i.e.*, the genes required for the growth of the organism.[8,11–14,16] Essential genes constitute potential drug targets, especially if they do not have any homologous counterparts in the human genome.[16,17]

*Biotechnology HPC Software Applications Institute, Telemedicine and Advanced Technology Research Center, U.S. Army Medical Research and Materiel Command, Ft. Detrick, MD 21702, USA.*
*E-mail: jaques.reifman@us.army.mil; Fax: +1 301-619-1983;*
*Tel: +1 301-619-7915*

† Electronic supplementary information (ESI) available: Sections S1, S2, and S3, the developed *iNJ*661i network in the Systems Biology Markup Language format (iNJ661i.xml), and the evaluation of potential synergy for all enzymes in the network in conjunction with 3-NP inhibition. See DOI: 10.1039/c1mb05106g



This journal is © The Royal Society of Chemistry 2011

# Report Documentation Page

*Form Approved*
*OMB No. 0704-0188*

Public reporting burden for the collection of information is estimated to average 1 hour per response, including the time for reviewing instructions, searching existing data sources, gathering and maintaining the data needed, and completing and reviewing the collection of information. Send comments regarding this burden estimate or any other aspect of this collection of information, including suggestions for reducing this burden, to Washington Headquarters Services, Directorate for Information Operations and Reports, 1215 Jefferson Davis Highway, Suite 1204, Arlington VA 22202-4302. Respondents should be aware that notwithstanding any other provision of law, no person shall be subject to a penalty for failing to comply with a collection of information if it does not display a currently valid OMB control number.

| 1. REPORT DATE | 2. REPORT TYPE | 3. DATES COVERED |
|---|---|---|
| **MAR 2011** | | **00-00-2011 to 00-00-2011** |

| 4. TITLE AND SUBTITLE | 5a. CONTRACT NUMBER |
|---|---|
| **Modeling synergistic drug inhibition of Mycobacterium tuberculosis growth in murine macrophages** | 5b. GRANT NUMBER |
| | 5c. PROGRAM ELEMENT NUMBER |
| 6. AUTHOR(S) | 5d. PROJECT NUMBER |
| | 5e. TASK NUMBER |
| | 5f. WORK UNIT NUMBER |
| 7. PERFORMING ORGANIZATION NAME(S) AND ADDRESS(ES)<br>**U.S. Army Medical Research and Materiel Command,Biotechnology High Performance Computing Software Applications Institute,Telemedicine and Advanced Technology Research Center,Fort Detrick,MD,21702** | 8. PERFORMING ORGANIZATION REPORT NUMBER |
| 9. SPONSORING/MONITORING AGENCY NAME(S) AND ADDRESS(ES) | 10. SPONSOR/MONITOR'S ACRONYM(S) |
| | 11. SPONSOR/MONITOR'S REPORT NUMBER(S) |

12. DISTRIBUTION/AVAILABILITY STATEMENT
**Approved for public release; distribution unlimited**

13. SUPPLEMENTARY NOTES

14. ABSTRACT

15. SUBJECT TERMS

| 16. SECURITY CLASSIFICATION OF: | | | 17. LIMITATION OF ABSTRACT | 18. NUMBER OF PAGES | 19a. NAME OF RESPONSIBLE PERSON |
|---|---|---|---|---|---|
| a. REPORT | b. ABSTRACT | c. THIS PAGE | | | |
| **unclassified** | **unclassified** | **unclassified** | **Same as Report (SAR)** | **15** | |

One important application of metabolic network modeling is the ability to quantitatively model metabolic enzyme inhibition and predict bacterial growth inhibition within *in vitro* media.[18] By integrating enzyme inhibition kinetics, metabolic network analysis, and cellular growth dynamics, we previously developed a systems biology framework that allow us to quantitatively reproduce the dose response of 3-nitropropionate (3-NP) on the growth of *M. tuberculosis* in a medium with the fatty acid propionate used as its carbon source. Similarly, we modeled the growth inhibition of *M. tuberculosis* by 5′-*O*-(*N*-salicyl-sulfamoyl)adenosine in a medium with a low iron concentration. Both studies used *in vitro* media modified to capture some characteristic feature of the *in vivo* environment, *i.e.*, restricted carbon sources and low ambient iron concentrations. One such specific *in vivo* environment is the macrophage.

In the early stages of infection, *M. tuberculosis* bacteria are typically localized in macrophage cells[19] where they survive host defense responses by multiple mechanisms, including blocking phagosomal maturation and countering host-induced antimicrobial peptides.[20,21] Part of the survival strategy involves metabolism, in particular, adaptation to the restricted availability of nutrients in the intracellular macrophage environment.[19,22]

When administering antibiotic treatments, it is essential to achieve the therapeutic antibiotic concentration at the site of action.[23,24] For TB treatments targeting intracellular *M. tuberculosis*, the drugs need to reach the immature phagosome in the macrophages, where the pathogen can persist for long times.[19,23–26] However, there are no studies that directly address the relationship between applied drug concentrations and the drug concentration in the cell compartment occupied by the pathogen. To understand the relationship between the applied drug dose and the actual intracellular concentration of the drug,[27,28] researchers are exploring mechanisms that enable drug transport across cell boundaries[27,29,30] to ascertain the effective drug concentrations in macrophages.[31,32] If therapeutic concentrations at the site of action cannot be achieved at clinically relevant concentrations, the drug will not be efficacious and might instead speed up the appearance of drug-resistant pathogens.

Drug combinations aim to increase therapeutic efficacies and reduce pharmacological liabilities over single drug treatments.[33,34] For example, the addition of the proposed TB drug SQ109 to isoniazid (commercially available as Laniazid or Nydrazid) improves the growth inhibition of *M. tuberculosis* beyond what either drug can achieve singly.[35] Modeling studies of multiple inhibitions of metabolic reactions can potentially provide a rapid means to identify suitable targets that can be proposed for developing drug combination therapies.[36] In this spirit, Lehar and co-workers used *in silico* analyses to examine the effect of inhibiting multiple reactions in a small hypothetical network that included parallel and serial reactions as well as reaction feedback loops.[37] This group also examined shifts in synergy among drug combinations targeting metabolic pathways in *Escherichia coli* under fermentation and aerobic conditions.[38] However, to fully realize the potential of using systems biology tools to investigate drug combinations for intracellular pathogens, we need to develop quantitative models that can account for multiple metabolic inhibitors at different doses and to account for the host environment where the pathogen resides.

In this study, we have begun addressing these issues by creating a systems biology framework capable of simulating the inhibitory effects of 3-NP on the intracellular growth of *M. tuberculosis*. We developed a metabolic network that could mimic the growth of *M. tuberculosis* in murine macrophages, derived the effective relationship between the intracellular and extracellular 3-NP concentrations surrounding the pathogen, and quantitatively modeled 3-NP inhibition under different biological conditions. We used the developed framework to study the properties of potential drug combinations targeting metabolic enzymes/pathways and found that the different carbon-utilization strategies of the pathogen in the macrophage creates distinct patterns of synergistic drug targets. Optimal growth inhibition in this system could be achieved by jointly targeting isocitrate lyases in the glyoxylate shunt and the glycerol utilization pathway, an effect that could not be captured in an *in vitro* model. To our knowledge, this is the first attempt to use metabolic networks in a comprehensive analysis of the dose-dependent effects of drug combinations on a pathogen's growth in host cells.

## Experimental

We have previously developed the systems biology framework required to simulate *in vitro* drug-induced growth inhibition of *M. tuberculosis*. We applied this technology to model the growth inhibition due to 3-NP in medium containing propionate, an odd-chained fatty acid, as the primary carbon source.[18] Here, we describe the extensions of this framework to model drug-induced growth inhibition of *M. tuberculosis* in macrophages.[39]

### Mathematical framework

Fig. 1 shows the general framework and relationship between our three model components, namely, the inhibition model, the metabolic network, and the population growth model. Each component deals with one specific aspect of modeling drug inhibition. The inhibition model (Inhibition Model) defines how a particular inhibitor affects the flux(es) of one or more metabolic reactions by creating inhibitor concentration-dependent constraints on each reactions, referred to as a "target reaction." The metabolic network (Metabolic Network) component accounts for how the changes in the metabolite fluxes of the target reactions decrease the biomass production rate of the organism. The population growth model (Population Growth Model) uses the reduced biomass production rate to estimate the bacterial cell concentration under these conditions. With these model components in place, we can map a specific inhibitor concentration inside macrophages $[I]_i$ (the subscript "*i*" denotes intracellular concentration) to a cell concentration $[X]$ as a function of time. This allows us to create dose-response curves and estimate minimum inhibitory concentrations in different media.

Although each of these components includes major differences compared to our previous *in vitro* model,[18] the main difference in the current framework formulation is that we did not explicitly account for the nutrient depletion in the macrophage. Instead, we assumed that the availability of

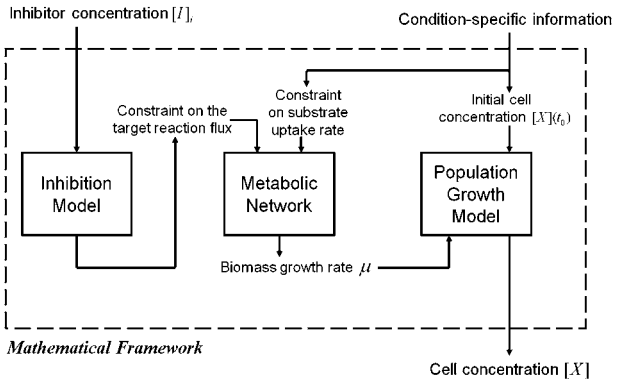


**Fig. 1** Mathematical framework: a set of coupled models used to simulate an inhibitor's effect on the growth of bacteria in host cells. Given the inhibitor concentration $[I]_i$, the inhibition model describes how the inhibitor affects the flux of the reaction(s) being inhibited [*i.e.*, the target reaction(s)]. These effects are modeled *via* explicit constraints on the target reaction flux(es). Using these constraints and constraints on the substrate uptake rate, we analyzed the metabolic network to infer the biomass production rate $\mu$. Using the population growth model, we related the biomass production rate $\mu$ to cell concentration $[X]$. Once these model components were specified, together with the constraints on the substrate uptake rates and the initial cell concentrations $[X](t_0)$ in host cells, the calculations performed within this framework only required input in the form of a specific inhibitor concentration $[I]_i$ to predict cellular growth. Here, the inhibitor concentration $[I]_i$ indicates the concentration of the inhibitor inside the macrophage and the subscript "*i*" denotes intracellular concentration.

nutrients/substrates taken up from the host cell did not change within the time frame of our study. In effect, this amounts to assuming that nutrient depletion was not the major cause for growth inhibition of the pathogen inside the macrophage. Given the relatively short time frame modeled in this study (less than 7 days) and that in the presence of an inhibitor bacterial growth slows down, effectively reducing the consumption of nutrients,[40] this assumption should be reasonably valid within this study. Thus, we did not dynamically change the constraints on the bacterial uptake rates as a function of time.

In order to capture the essential metabolic components of *M. tuberculosis*-infected mouse macrophage cells growing in a drug-infused medium,[39] we assumed that the pathogen resides in the phagosome compartment and uses lipids, composed of fatty acids and glycerol, as carbon sources. The 3-NP drug molecules in the medium are taken up by the macrophage, enter the phagosome, and retard *M. tuberculosis* growth by inhibiting two essential metabolic reactions required to use fatty acids, isocitrate lyase (ICL) and methylisocitrate lyase (MCL):[39]

$$\text{ICL: isocitrate} \rightarrow \text{succinate} + \text{glyoxylate} \qquad (1)$$

$$\text{MCL: methylisocitrate} \rightarrow \text{succinate} + \text{pyruvate} \qquad (2)$$

These reactions are each catalyzed by the enzymes isocitrate lyase 1 (ICL1) and isocitrate lyase 2 (ICL2), encoded by the *icl1* and *icl2* genes, respectively.[41,42] Because these reactions do not have any mammalian counterparts, 3-NP has no observable effects on the activity of macrophages.[39] Thus, in Fig. 1, the inhibitor corresponds to 3-NP, the inhibitor concentration $[I]_i$ refers to the 3-NP concentration in the phagosome $[\text{3-NP}]_i$, the target reactions are the above ICL and MCL reactions, and the biomass production rate $\mu$ and cell concentration $[X]$ are those of *M. tuberculosis*. The details of the inhibition model, metabolic network, and population growth model are given below.

### Inhibition model

This model describes the inhibitor concentration-dependent constraints on the metabolic reaction fluxes in the metabolic network simulations. Since the enzymatic inhibition mechanism remains the same under *in vitro* and *ex vivo* conditions, we used the previous inhibition model[18] except that the inhibitor concentration now refers to the intracellular phagosome 3-NP concentration ($[\text{3-NP}]_i$). Thus, the ratio of inhibitor-present to inhibitor-free fluxes for the ICL reaction ($f_{\text{ICL}}$) is as follows:

$$\begin{aligned} f_{\text{ICL}}([\text{3-NP}]_i) &= \frac{\nu_{\text{ICL}}}{\nu_{\text{ICL,WT}}} \\ &= w_{\text{ICL1}} \frac{1+\frac{[\text{SUC}]}{K_{\text{SUC,ICL1}}}}{1+\frac{[\text{SUC}]}{K_{\text{SUC,ICL1}}}+\frac{[\text{3-NP}]_i}{K_{\text{3-NP,ICL1}}}} \\ &\quad + w_{\text{ICL2}} \frac{1+\frac{[\text{SUC}]}{K_{\text{SUC,ICL2}}}}{1+\frac{[\text{SUC}]}{K_{\text{SUC,ICL2}}}+\frac{[\text{3-NP}]_i}{K_{\text{3-NP,ICL2}}}} \end{aligned} \qquad (3)$$

where $\nu_{\text{ICL}}$ and $\nu_{\text{ICL,WT}}$ denote the inhibitor-present and inhibitor-free reaction fluxes, respectively, the "*i*" in $[\text{3-NP}]_i$ denotes intracellular concentrations, $w_{\text{ICL1}}$ and $w_{\text{ICL2}}$ denote the fractions of the overall inhibitor-free ICL reaction flux for the reaction parts catalyzed by enzymes ICL1 and ICL2, respectively, SUC denotes the succinate substrate; [SUC] indicates its concentration, and $K_{\text{3-NP,ICL1}}$, $K_{\text{3-NP,ICL2}}$, $K_{\text{SUC,ICL1}}$, and $K_{\text{SUC,ICL2}}$ denote Michaelis constants.[43] Similarly, the ratio for the MCL reaction ($f_{\text{MCL}}$) is as follows:

$$\begin{aligned} f_{\text{MCL}}([\text{3-NP}]_i) &= \frac{\nu_{\text{MCL}}}{\nu_{\text{MCL,WT}}} \\ &= w_{\text{MCL1}} \frac{1+\frac{[\text{SUC}]}{K_{\text{SUC,MCL1}}}}{1+\frac{[\text{SUC}]}{K_{\text{SUC,MCL1}}}+\frac{[\text{3-NP}]_i}{K_{\text{3-NP,MCL1}}}} \\ &\quad + w_{\text{MCL2}} \frac{1+\frac{[\text{SUC}]}{K_{\text{SUC,MCL2}}}}{1+\frac{[\text{SUC}]}{K_{\text{SUC,MCL2}}}+\frac{[\text{3-NP}]_i}{K_{\text{3-NP,MCL2}}}} \end{aligned} \qquad (4)$$

where the variables and parameters have similar definitions to those in eqn (3). The parameter values in eqn (3) and (4) are the same as those used in the *in vitro* inhibition model.[18]

### Metabolic network

The metabolic network model was used to calculate the biomass production rate $\mu$ (in $\text{h}^{-1}$), which was subject to the constraint in the flux of each target reaction modeled in eqn (3) and (4). We modified the metabolic network to account for the unique metabolic conditions that the pathogen encounters in the macrophage cells. As a starting point, we used the previously developed *iNJ*661v model to represent the metabolic

 This journal is © The Royal Society of Chemistry 2011

**Table 1** Modifications of the *iNJ*661v metabolic network to obtain the *iNJ*661i network. To develop a network compatible with the metabolism of *Mycobacterium tuberculosis* in cultivated mouse macrophage cells, we modified an existing *in vivo* network, *iNJ*661v,[44] by reducing the inconsistencies between the predicted gene essentiality and the essentiality experimentally measured in mouse macrophage cells.[47] We first corrected six inconsistencies between *iNJ*661v-predicted and experimental gene essentiality (for the *Rv0098*, *fadD21*, *plsC*, *Rv3588c*, *desA3*, and *kefB* genes) by restoring several enzyme functions and reactions disabled in *iNJ*661v and then, through a set of systematic optimization procedures,[44,46] further corrected 13 inconsistencies

| Index | Gene locus | Gene name | Essentiality measured in experiment | Essentiality predicted from *iNJ*661v | Essentiality predicted from *iNJ*661i | Modification to correct the inconsistency between the experimental and predicted gene essentiality |
|---|---|---|---|---|---|---|
| 1 | *Rv0098* | *Rv0098* | Non-essential | Essential | Non-essential | Restored the disabled ability of the product of the *fabG1* gene to catalyze mycolic acid synthesis |
| 2 | *Rv1185c* | *fadD21* | Non-essential | Essential | Non-essential | Restored the disabled ability of the products of the *fadD9*, *fadD24*, and *fadD23* genes to function as fatty acid-CoA ligase |
| 3 | *Rv2483c* | *plsC* | Non-essential | Essential | Non-essential | Restored the disabled ability of the product of the *Rv2182c* gene to function as 1-hexadecanoyl-sn-glycerol 3-phosphate *O*-acyltransferase |
| 4 | *Rv3588c* | *Rv3588c* | Non-essential | Essential | Non-essential | Restored the disabled ability of the product of the *Rv3273* gene to catalyze carboxylic acid dissociation and association |
| 5 | *Rv3229c* | *desA3* | Non-essential | Essential | Non-essential | Restored the disabled synthesis of hexadecenoate |
| 6 | *Rv3236c* | *kefB* | Non-essential | Essential | Non-essential | Restored the disabled ion transports by the potassium ABC transporter and sodium proton antiporter |
| 7 | *Rv1092c* | *coaA* | Non-essential | Essential | Non-essential | Deleted pantetheine 4′-phosphate from the biomass objective function |
| 8 | *Rv1653* | *argJ* | Non-essential | Essential | Non-essential | Allowed the uptakes of ornithine and arginine |
| 9 | *Rv2210c* | *ilvE* | Non-essential | Essential | Non-essential | Allowed the uptake of leucine |
| 10 | *Rv2388c* | *hemN* | Non-essential | Essential | Non-essential | Deleted protoheme from the biomass objective function |
| 11 | *Rv2573* | *Rv2573* | Non-essential | Essential | Non-essential | Deleted pantetheine 4′-phosphate from the biomass objective function |
| 12 | *Rv2702* | *ppgK* | Non-essential | Essential | Non-essential | Allowed fluxes through the reactions catalyzed by maltose trehalose isomerase and α-glucosidase |
| 13 | *Rv2945c* | *lppX* | Non-essential | Essential | Non-essential | Deleted extracellular phthiocerol dimycocerosate A and phenol phthiocerol dimycocerosate from the biomass objective function |
| 14 | *Rv2949c* | *Rv2949c* | Non-essential | Essential | Non-essential | Allowed the uptake of phenol palmitic acid |
| 15 | *Rv2977c* | *thiL* | Non-essential | Essential | Non-essential | Deleted thiamin from the biomass objective function |
| 16 | *Rv2995c* | *leuB* | Non-essential | Essential | Non-essential | Added the uptakes of leucine |
| 17 | *Rv3340* | *metC* | Non-essential | Essential | Non-essential | Changed the reaction catalyzed by the cystathionine β-synthase enzyme into reversible |
| 18 | *Rv0503c* | *cmaA2* | Essential | Non-essential | Essential | Blocked the ability of the product of the *mmaA2* gene to catalyze mycolic acid cyclopropanation |
| 19 | *Rv0820* | *phoT* | Essential | Non-essential | Essential | Blocked the phosphate uptake through diffusion and blocked the ability of the product of the *pstA2* gene to catalyze the phosphate uptake *via* the ABC system |

state of *M. tuberculosis* in whole animals[44] (see Section S1 in the ESI† for details on the network model selection). Next, we used gene essentiality data to modify[44–46] this network by reducing the inconsistencies between the network-predicted gene essentiality and those experimentally validated for *M. tuberculosis* cells growing in murine macrophages.[47] We first corrected six discrepancies between the *iNJ*661v-predicted and experimental essentiality by restoring several enzyme functions and reactions disabled in *iNJ*661v and then, through a set of systematic optimization procedures,[44,46] further corrected 13 wrong predictions (see Table 1). The resultant network, *iNJ*661i, did not change the role of fatty acids and glycerol as major carbon sources, consistent with the experimental observation that these molecules are the main carbon sources for *M. tuberculosis* in both whole animals and cultivated macrophages.[39]

We then refined the constraints on the substrate uptakes of *iNJ*661i, focusing on the role of carbon metabolism.[39] Based on the experimental observation that the limitations associated with carbon metabolism determine the growth of *M. tuberculosis*,[39] we left all non-carbon-containing metabolite uptakes unconstrained. As fatty acids and glycerol are the major carbon sources,[19,39] we allowed all uptakes of these metabolites. The upper limits of the fatty acid uptakes ($U_{\mathrm{Fat}}$) and the glycerol uptake ($U_{\mathrm{Glyc}}$) were determined by matching our model calculation with experimentally determined *M. tuberculosis* cell concentrations. As for other carbon-containing substrates (arginine, cytidine, isoleucine, leucine, ornithine, phenol palmitic acid, tyrosine, valine, and xylose), we decreased the upper limits of their uptakes ($U_{\mathrm{C}}$) to a small value [0.005 mmol $h^{-1}$ g dry $wt^{-1}$ (*i.e.*, 0.005 millimoles per hour per gram dry weight of *M. tuberculosis*)] below which they generated new false predictions of gene essentiality. We provide the developed *iNJ*661i network in Systems Biology Markup Language format in the ESI.† Compared with the network used in our previous *in vitro* study,[18] the *iNJ*661i network included the uptakes of more substrates, including glycerol, fatty acids other than propionate, nitrate, and the above listed other carbon-containing substrates.

Finally, we performed FBA of the *iNJ*661i metabolic network using the COBRA Toolbox[48] to calculate *M. tuberculosis* biomass production rates ($\mu$) with different sets of constraints on the target reaction fluxes. We calculated the biomass production rate of wild-type *M. tuberculosis* in the absence of the 3-NP inhibitor by leaving the ICL and MCL reaction fluxes unconstrained. In this case, after FBA, we also used the COBRA Toolbox[48] to minimize the sum of reaction fluxes while keeping the calculated maximal biomass growth rate. This procedure allowed us to obtain a unique set of minimum inhibitor-free fluxes for all reactions, including $\nu_{\mathrm{ICL,WT}}$ and $\nu_{\mathrm{MCL,WT}}$ for the ICL and MCL reactions, respectively, corresponding to the most parsimonious flow of metabolites through the network.[49–51]

We calculated the biomass production rate in the presence of 3-NP by constraining the flux of the ICL and MCL reactions, respectively, to be no more than the product of the flux ratios $f_{\mathrm{ICL}}$ and $f_{\mathrm{MCL}}$, calculated from eqn (3) and (4), and the inhibitor-free fluxes $\nu_{\mathrm{ICL,WT}}$ and $\nu_{\mathrm{MCL,WT}}$. That is, the upper limit of the flux through the ICL (or MCL) reaction was $f_{\mathrm{ICL}}\nu_{\mathrm{ICL,WT}}$ (or $f_{\mathrm{MCL}}\nu_{\mathrm{MCL,WT}}$). We calculated the biomass production rate of the deletion mutant Δ*icl1*Δ*icl2* of *M. tuberculosis* by setting the fluxes of the target reactions ICL and MCL to zero. In cases where we explored potential drug combinations with 3-NP, we not only limited the ICL and MCL reaction fluxes but also constrained the reaction flux associated with the other putative target enzyme.

Under each particular set of conditions and constraints, we calculated $\mu$ and used the population growth model to estimate the time-dependent cell concentrations of *M. tuberculosis*.

### Population growth model

We used a population growth model to calculate the *M. tuberculosis* concentration [*X*] as a function of time *t*, using the biomass production rate $\mu$ determined from FBA of the metabolic network. This model was an extension of the earlier *in vitro* population model[18] in that it accounted for the elimination of pathogen cells by the macrophage.[52] It also accounted for a delay in the onset of bacterial growth by including an initial lag phase in which bacterial cells are still adapting to the environment and not multiplying.[53] These features were captured by the population growth model by including the macrophage bacterial lysis rate ($k_d$) and two different equations for the bacterial growth within and after the lag stage, respectively.

Let *t* represent time and $\tau$ the time point at which the lag stage ends. Thus, $t \leq \tau$ indicates time within the lag stage, and $t > \tau$ indicates time after the lag stage. Therefore, the growth population model is as follows:

$$\frac{\mathrm{d}[X]}{\mathrm{d}t} = -24k_d[X] \quad \text{at } t \leq \tau \tag{5}$$

$$\frac{\mathrm{d}[X]}{\mathrm{d}t} = 24(\mu - k_d)[X] \text{ at } t > \tau \tag{6}$$

where *t* and $\tau$ are measured in units of days, [*X*] represents the cell concentration [in colony-forming units (CFUs)], the factor of 24 converts the units of time *t* from hours to days, and $k_d$ represents the bacterial lysis rate (in $h^{-1}$). We set the value of $k_d$ to 0.015 $h^{-1}$, which is compatible with the largest experimental decline of cell concentrations of *M. tuberculosis* in the mouse macrophage.[39] Eqn (5) indicates that cell concentrations could decrease as a function of time during the lag stage. This allowed us to model a possible "pause" in bacterial growth brought on by the change in environment, *i.e.*, bacterial entry into a macrophage, yet still permitted macrophage-induced cell killing. Such initial decrease in cell concentrations of intracellular bacteria during the lag stage has also been experimentally observed in other intracellular pathogens, *e.g.*, for *Legionella pneumophila* taken up by *Acanthamoeba castellanii* cells.[53] To make the calculation results comparable with the experimental data, we integrated eqn (5) and (6) and converted the resultant natural logarithms into common logarithms as follows:

$$\log_{10}[X](t) = \log_{10}[X](t_0) - 24k_d\,(t - t_0)/2.303 \text{ at } t \leq \tau \tag{7}$$

$$\log_{10}[X](t) = \log_{10}[X](\tau) + 24(\mu - k_d)(t - \tau)/2.303 \text{ at } t > \tau \tag{8}$$

where $t_0$ represents the initial time, which based on the experimental data was set to 1 day.[39] The calculated cell concentrations [*X*] in eqn (7) and (8) were then directly compared with the experimental data.

### Sensitivity analysis

The presence of a number of parameters in our mathematical framework warranted a sensitivity analysis to ascertain how the assigned parameter values affected the final computational results. Table 2 shows a summary of all parameters used to construct the computational framework. To address sensitivity issues for different types of parameters, we classified the parameters into three groups: (1) those obtained from the literature (*group I*), (2) those determined by matching experimental data (fitted parameters) (*group II*), and (3) those that, by

 This journal is © The Royal Society of Chemistry 2011

**Table 2** Parameters of the mathematical framework used to model intracellular cell growth inhibition by 3-nitropropionate (3-NP). *Group I* included parameters obtained from the literature, *group II* included parameters determined by matching the experimental data, and *group III* included parameters that by definition were derived from other parameters (dependent parameters)

| Group | Parameter | Model | Equation(s) | Value | Source |
|---|---|---|---|---|---|
| I | [SUC] | Inhibition model | 3 and 4 | $2.5 \times 10^{0}$ mM | Fang *et al.*[18] |
| | $K_{SUC,ICL1}$ | Inhibition model | 3 | $1.5 \times 10^{0}$ mM | Fang *et al.*[18] |
| | $K_{SUC,MCL1}$ | Inhibition model | 4 | $1.5 \times 10^{0}$ mM | Fang *et al.*[18] |
| | $K_{SUC,ICL2}$ | Inhibition model | 3 | $1.5 \times 10^{1}$ mM | Fang *et al.*[18] |
| | $K_{SUC,MCL2}$ | Inhibition model | 4 | $1.5 \times 10^{1}$ mM | Fang *et al.*[18] |
| | $K_{3\text{-NP,ICL1}}$ | Inhibition model | 3 | $3.0 \times 10^{-3}$ mM | Fang *et al.*[18] |
| | $K_{3\text{-NP,MCL1}}$ | Inhibition model | 4 | $3.0 \times 10^{-3}$ mM | Fang *et al.*[18] |
| | $K_{3\text{-NP,ICL2}}$ | Inhibition model | 3 | $1.1 \times 10^{-1}$ mM | Fang *et al.*[18] |
| | $K_{3\text{-NP,MCL2}}$ | Inhibition model | 4 | $1.1 \times 10^{-1}$ mM | Fang *et al.*[18] |
| | $w_{ICL1}$ | Inhibition model | 3 | $7.9 \times 10^{-1}$ | Fang *et al.*[18] |
| | $w_{MCL1}$ | Inhibition model | 4 | $1.0 \times 10^{0}$ | Fang *et al.*[18] |
| | $U_C$ | Metabolic network | — | $5.0 \times 10^{-3}$ mmol $h^{-1}$ g dry $wt^{-1}$ | Fang *et al.*[44] |
| | $k_d$ | Population growth model | 7 and 8 | $1.5 \times 10^{-2}$ $h^{-1}$ | Munoz-Elias *et al.*[39] |
| | $\log_{10}[X](t_0)$ | Population growth model | 7 | — | Munoz-Elias *et al.*[39] |
| II | $U_{Fat}$ | Metabolic network | — | — | Obtained by matching |
| | $U_{Glyc}$ | Metabolic network | — | — | experimental cell |
| | $\tau$ | Population growth model | 7 and 8 | — | growth data[39] |
| III | $w_{ICL2}$ | Inhibition model | 3 | — | Equal to 1-$w_{ICL1}$ |
| | $w_{MCL2}$ | Inhibition model | 4 | — | Equal to 1-$w_{MCL1}$ |

definition, were derived from other parameters, *i.e.*, dependent parameters (*group III*).

We estimated the relationship between the computational result and the corresponding parameter by calculating the sensitivity coefficient for the parameter. For example, if $\log_{10}[X]$ represents the common logarithm of cell concentration (in CFUs) and $p$ represents the parameter being analyzed, the sensitivity coefficient ($S_p$) is defined as follows:[54,55]

$$S_p = \frac{\partial(\log_{10}[X])/(\log_{10}[X])}{\partial p/p} \quad (9)$$

We numerically estimated the sensitivity coefficient $S_p$ for parameter $p$ by starting from $\partial p = +0.5p$ and repeating the process of reducing $\partial p$ and calculating $S_p$ until the value of $S_p$ converged. We then repeated the process starting from $\partial p = -0.5p$ until convergence. In the calculations performed here, both processes converged to the same numerical value. We only performed sensitivity analysis for the parameters in *groups I* and *II*, as the variations in the dependent parameters in *group III* were, by definition, implicitly considered in these analyses.

## Results and discussion

### Simulation of growth inhibition of *M. tuberculosis* in macrophage cells

Munoz-Elias and McKinney used *M. tuberculosis*-infected mouse macrophage cells to quantify intracellular pathogen growth during a six-day period in defined media with and without 3-NP.[39] The Munoz-Elias and McKinney study consists of three independent experiments that compare: (1) growth of the Δ*icl1*Δ*icl2* deletion mutant strain with wild-type *M. tuberculosis*; (2) growth of *M. tuberculosis* with 10.0 mM 3-NP present in the medium compared with the inhibitor-free condition; and (3) growth of *M. tuberculosis* with 0.2, 1.0, and 5.0 mM 3-NP in the medium compared with the inhibitor-free condition. Note that the cited 3-NP concentrations in the medium correspond to extracellular concentrations rather than the intracellular concentrations present in the phagosome compartment.

We used the mathematical framework shown in Fig. 1 to attempt to reproduce the results from the above experiments. We performed eight distinct simulations to mimic the growth data for eight different conditions in the above experimental study (see Table 3). For each condition, we simulated the growth of a particular strain of *M. tuberculosis* (wild-type or the Δ*icl1*Δ*icl2* deletion mutant) under a distinct extracellular 3-NP concentration by setting the initial cell concentration $[X](t_0)$ to the measured value at *day 1* and fitting growth data to the experimental cell concentrations at *days 4* and *7* to estimate one or two other parameter values.[39] These parameters included the time $\tau$ at which the lag stage ends, the upper limit of the glycerol uptake ($U_{Glyc}$), the upper limit of fatty acid uptake ($U_{Fat}$), and the intracellular 3-NP concentration ($[3\text{-NP}]_i$). We determined the value for $\tau$ for each condition, set the uptake limits $U_{Glyc}$ and $U_{Fat}$ in the simulations for *Conditions 1* and *2*, respectively, and obtained the intracellular 3-NP concentrations $[3\text{-NP}]_i$ in the simulation for *Conditions 4–7* (see Section S2 in the ESI† for details).

Fig. 2A–C, shows the simulated cell concentrations of (1) wild-type *M. tuberculosis* and the Δ*icl1*Δ*icl2* deletion mutant; (2) *M. tuberculosis* with and without 10.0 mM 3-NP in the medium; and (3) *M. tuberculosis* with and without 0.2, 1.0, and 5.0 mM 3-NP in the medium. Table 3 shows the root mean squared error (RMSE) between the simulated and experimental cell concentrations in $\log_{10}$ units. In general, the simulated cell concentrations were in close agreement with the experimental data, with a RMSE of less than 0.07. The exception is shown in Fig. 2C, where, in the absence of 3-NP, the simulated cell concentration at *day 7* was higher than the corresponding experimental data, with a RMSE of 0.20. The predicted higher cell concentrations stemmed from our assumption that the substrate uptake rates of *M. tuberculosis* inside the phagosome do not change with time. For drug-induced growth-retarded bacteria, this is an adequate assumption for the time period modeled, but for unrestricted growth, this assumption can introduce errors at *days 5* to *7*.

**Table 3** The procedure used to determine parameter values and reproduce experimental cell concentrations of *Mycobacterium tuberculosis*. We performed eight distinct simulations to attempt to reproduce the growth data for eight different conditions in an experimental study[39] (see Section S2 in the ESI† for details). For each condition, we simulated the growth of a particular *M. tuberculosis* strain under a distinct extracellular 3-nitropropionate (3-NP) concentration ($[3\text{-NP}]_e$, where the subscript "*e*" denotes extracellular concentration) by setting the initial cell concentration $[X](t_0)$ to the measured value at *day 1* and fitting growth data to the experimental cell concentrations at *days 4* and *7* to estimate one or two other parameter values.[39] The parameters obtained in the simulations for *Conditions 1* and *2* were, in turn, used in the simulations of other conditions. The root mean squared error (RMSE) indicates the difference between the common logarithms of the simulation results and experimental cell concentration values. $[3\text{-NP}]_i$ represents the intracellular 3-NP concentration, where the subscript "*i*" denotes intracellular concentration. $U_{Fat}$ and $U_{Glyc}$ represent the upper limits of the uptake rates of fatty acids and glycerol, respectively [in millimoles per hour per gram dry weight of *M. tuberculosis* (*i.e.*, mmol $h^{-1}$·g dry $wt^{-1}$)]. $\tau$ represents the time at the end of the lag stage. $[X](t_0)$ denotes the initial cell concentration of *M. tuberculosis* [in colony-forming units (CFU)]. $k_d$ represents the lysis rate of *M. tuberculosis* cells. The 11 parameters of the inhibition model are those in eqn (3) and (4) in the Experimental Section. RMSE = $\{[\sum_{t=1,4,7}\{\log_{10}[X]_{sim}(t) - \log_{10}[X]\exp(t)\}^2]/N\}^{1/2}$, where $[X]_{sim}$ and $[X]_{exp}$ denote the simulated and experimentally measured cell concentrations, respectively; *t* represents time; and *N* denotes the number of data points ($N = 3$)

| Condition Index | Strain | $[3\text{-NP}]_e$ (mM) | Parameters from the literature | Parameters determined in this condition | Parameters from previous conditions | Figure | RMSE |
|---|---|---|---|---|---|---|---|
| 1 | Δ*icl1*Δ*icl2* | 0.0 | $[X](t_0) = 10^{3.95}$ CFU, $k_d$ | $\tau$ = 4.0 day, $U_{Glyc}$ = 0.041 mmol $h^{-1}$ g dry $wt^{-1}$ | — | 2A | 0.001 |
| 2 | Wild-type | 0.0 | $[X](t_0) = 10^{3.95}$ CFU, $k_d$ | $\tau$ = 2.2 day, $U_{Fat}$ = 0.014 mmol $h^{-1}$ g dry $wt^{-1}$ | $U_{Glyc}$ from *Condition 1* | 2A | 0.001 |
| 3 | Wild-type | 0.0 | $[X](t_0) = 10^{4.10}$ CFU, $k_d$ | $\tau$ = 1.5 day | $U_{Glyc}$ from *Condition 1*, $U_{Fat}$ from *Condition 2* | 2B | 0.067 |
| 4 | Wild-type | 10.0 | $[X](t_0) = 10^{4.07}$ CFU, $k_d$ and 11 parameters of inhibition model | $\tau$ = 2.4 day, $[3\text{-NP}]_i$ = 0.118 mM | $U_{Glyc}$ from *Condition 1*, $U_{Fat}$ from *Condition 2* | 2B | 0.001 |
| 5 | Wild-type | 5.0 | $[X](t_0) = 10^{4.46}$ CFU, $k_d$ and 11 parameters of inhibition model | $\tau$ = 1.0 day, $[3\text{-NP}]_i$ = 0.063 mM | $U_{Glyc}$ from *Condition 1*, $U_{Fat}$ from *Condition 2* | 2C | 0.032 |
| 6 | Wild-type | 1.0 | $[X](t_0) = 10^{4.46}$ CFU, $k_d$ and 11 parameters of inhibition model | $\tau$ = 1.0 day, $[3\text{-NP}]_i$ = 0.023 mM | $U_{Glyc}$ from *Condition 1*, $U_{Fat}$ from *Condition 2* | 2C | 0.015 |
| 7 | Wild-type | 0.2 | $[X](t_0) = 10^{4.55}$ CFU, $k_d$ and 11 parameters of inhibition model | $\tau$ = 1.0 day, $[3\text{-NP}]_i$ = 0.012 mM | $U_{Glyc}$ from *Condition 1*, $U_{Fat}$ from *Condition 2* | 2C | 0.029 |
| 8 | Wild-type | 0.0 | $[X](t_0) = 10^{4.45}$ CFU | $\tau$ = 1.0 day | $U_{Glyc}$ from *Condition 1*, $U_{Fat}$ from *Condition 2* | 2C | 0.204 |

Our approach used a static description of nutrient uptakes from the host cell, *i.e.*, the potential dynamic responses of the host were not included. Eventually, we would like to include the time-dependent responses of host cells that influence the metabolism and growth of intracellular pathogens. The recent development of an integrated *M. tuberculosis*-macrophage metabolic model (*iAB-iAMØ*-1410-Mt-661)[56] provides the foundation for this effort, although much additional development will be needed to account for all relevant interactions between the host and the pathogen. Further extensions of the present work to incorporate these models and other biological network descriptions of signaling and regulatory networks will allow us to construct a more comprehensive description of drug-induced growth inhibition of intracellular pathogens.

To highlight the difference between our previously *in vitro*-derived framework[18] and the deployed macrophage-based framework derived here, we compared the abilities of the two models to reproduce the *ex vivo* wild-type and mutant growth data. Fig. 3 shows that, although the *in vitro* simulation results for wild-type *M. tuberculosis* could roughly match the experimental data, the simulated cell concentrations of the Δ*icl1*Δ*icl2* deletion mutant were inconsistent with the experimental data. To account for the macrophage action in the *in vitro* framework, we added the lysis rate ($k_d$) to the population growth model and re-simulated the growth of the Δ*icl1*Δ*icl2* deletion mutant. Fig. 3 shows that the simulation results from this modification improved the correspondence with the experimental data, but the results neither fully captured the experimental data nor the results derived from the intracellular macrophage model simulations, because the *in vitro* framework failed to predict a non-zero growth rate for the Δ*icl1*Δ*icl2* deletion mutant.

### Sensitivity analysis of the model parameters

To quantitatively measure how the parameter values affected the simulation results, we calculated the sensitivity coefficients $S_p$ for each of the parameters in *groups I* and *II* (Table 2) at different 3-NP concentrations in the medium. For this analysis, we used the simulation results shown in Fig. 2C at *day 4* as references, and, accordingly, $\log_{10}[X]$ in eqn (9) refers to the common logarithms of the calculated cell concentrations at that day. Table 4 shows the calculated sensitivity coefficient for each parameter at different extracellular 3-NP concentrations (0.0, 0.2, 1.0, and 5.0 mM). By construction, the parameters associated with the inhibition model had zero sensitivity in the absence of an inhibitor. Among the parameters in the metabolic network, the upper limit of fatty acids uptake ($U_{Fat}$) had a significantly higher sensitivity coefficient than that of glycerol uptake ($U_{Glyc}$), suggesting that, among major carbon sources, fatty acids were more important than glycerol for the growth of *M. tuberculosis*. The relatively low sensitivity associated with glycerol uptake was consistent with the experimental observation that in the presence of other carbon sources *M. tuberculosis* glycerol metabolism is not altered.[57] Thus, the observed fixed metabolic fate of glycerol indicated that

 This journal is © The Royal Society of Chemistry 2011

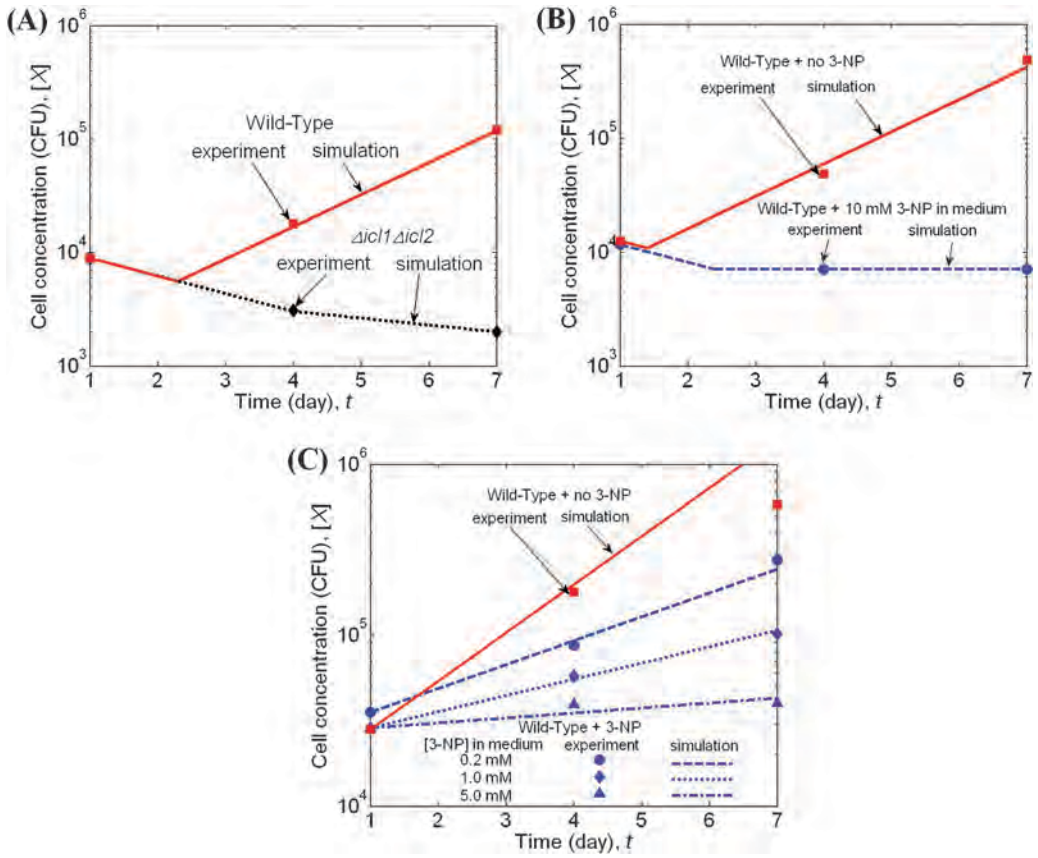


**Fig. 2** Simulation results and experimental data for the growth of *Mycobacterium tuberculosis* in the absence and presence of 3-nitropropionate (3-NP) inhibitor. Growth curves were compared between (A) wild-type *M. tuberculosis* cells and the Δ*icl1icl2* deletion mutant, (B) wild-type cells in medium with and without 10 mM 3-nitropropionate (3-NP), and (C) wild-type cells in medium with 3-NP concentrations of 0.2, 1.0, and 5.0 mM and without 3-NP. The experimental data were taken from the literature.[39] [*X*] represents the cell concentration of *M. tuberculosis*; *t* represents time. CFU, colony-forming units.

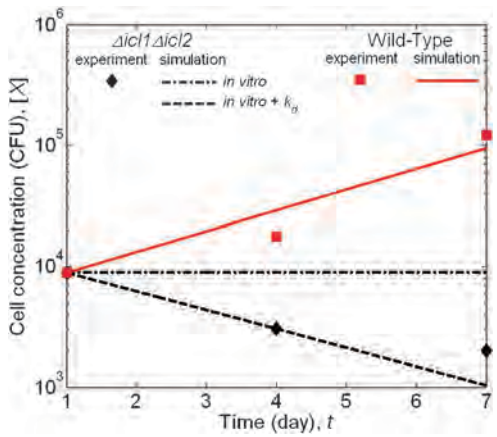


**Fig. 3** Simulation results of the growth of wild-type *Mycobacterium tuberculosis* cells and the Δ*icl1*Δ*icl2* deletion mutant using the previous *in vitro* framework. The solid line shows cell concentrations of wild-type cells calculated using the *in vitro* framework, the dotted-dashed line shows cell concentrations of the Δ*icl1*Δ*icl2* deletion mutant calculated using the *in vitro* framework, and the dashed line shows cell concentrations of the Δ*icl1*Δ*icl2* deletion mutant calculated using the *in vitro* framework with the lysis rate ($k_d$). The experimental data were taken from the literature.[39]

*M. tuberculosis* might be unable to adjust its glycerol metabolism to optimize growth. Instead, the organism might attempt to optimize its growth by adjusting its fatty acid metabolism, reinforcing the notion that, compared with glycerol, fatty acids might play a more important role in the growth of *M. tuberculosis* under limiting nutrient conditions. The relatively small sensitivity coefficient of the upper limit of the uptakes of other carbon-containing substrates ($U_C$) also indicated that fatty acids were more important than these substrates. For the parameters in the population growth model, the initial cell concentration, $\log_{10}[X](t_0)$, had a large sensitivity coefficient, as the initial cell concentration directly affects the concentrations at later time points. The lysis rate ($k_d$) had relatively small coefficients, suggesting that the lysis of the *M. tuberculosis* cells had a small influence on cell concentration. This lack of influence also propagated to small sensitivity coefficients for the lag time ($\tau$), as before this time only lysis affected the concentration of *M. tuberculosis*.

### Analysis of the relation between the intracellular and extracellular inhibitor concentrations

In the experiments, the extracellular 3-NP concentrations were set to 0.2, 1.0, 5.0, and 10.0 mM,[39] while, correspondingly, we

**Table 4** Sensitivity coefficients of the model parameters. Sensitivity coefficient $S_p = (\Delta\log_{10}[X]\cdot p)/(\Delta p\cdot\log_{10}[X])$, where $p$ represents the tested parameter and $[X]$ represents the cell concentration at *day 4* in Fig. 2C. $[3\text{-NP}]_e$ represents the extracellular 3-nitropropionate (3-NP) concentration. The inhibition model parameters are from eqn (3) and (4), whereas the population growth model parameters are from eqn (7) and (8)

| | | $[3\text{-NP}]_e$ | | | |
|---|---|---|---|---|---|
| Parameter | Model | 0.0 mM | 0.2 mM | 1.0 mM | 5.0 mM |
| [SUC] | Inhibition model | 0.000 | 0.030 | 0.028 | 0.016 |
| $K_{SUC,ICL1}$ | Inhibition model | 0.000 | −0.018 | −0.016 | −0.009 |
| $K_{SUC,MCL1}$ | Inhibition model | 0.000 | −0.012 | −0.011 | −0.006 |
| $K_{SUC,ICL2}$ | Inhibition model | 0.000 | 0.000 | −0.001 | −0.001 |
| $K_{SUC,MCL2}$ | Inhibition model | 0.000 | 0.000 | 0.000 | 0.000 |
| $K_{3\text{-NP,ICL1}}$ | Inhibition model | 0.000 | 0.028 | 0.026 | 0.014 |
| $K_{3\text{-NP,MCL1}}$ | Inhibition model | 0.000 | 0.020 | 0.018 | 0.010 |
| $K_{3\text{-NP,ICL2}}$ | Inhibition model | 0.000 | 0.003 | 0.005 | 0.009 |
| $K_{3\text{-NP,MCL2}}$ | Inhibition model | 0.000 | 0.000 | 0.000 | 0.000 |
| $w_{ICL1}$ | Inhibition model | 0.000 | −0.064 | −0.085 | −0.081 |
| $w_{MCL1}$ | Inhibition model | 0.000 | −0.045 | −0.060 | −0.057 |
| $U_{Fat}$ | Metabolic network | 0.224 | 0.125 | 0.104 | 0.062 |
| $U_{Glyc}$ | Metabolic network | 0.010 | 0.022 | 0.030 | 0.036 |
| $U_C$ | Metabolic network | 0.012 | 0.032 | 0.019 | 0.022 |
| $\log_{10}[X](t_0)$ | Population growth model | 0.842 | 0.916 | 0.947 | 0.984 |
| $k_d$ | Population growth model | −0.089 | −0.095 | −0.100 | −0.104 |
| $\tau$ | Population growth model | −0.082 | −0.059 | −0.051 | −0.040 |

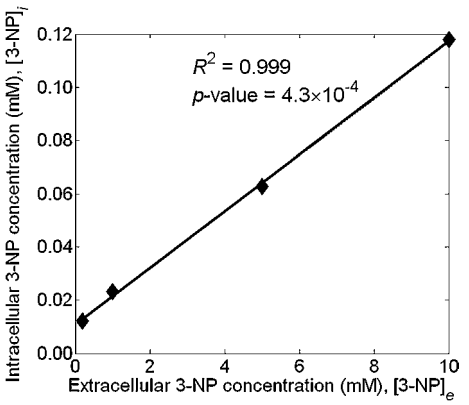


**Fig. 4** Relation between intracellular 3-nitropropionate (3-NP) concentrations and extracellular 3-NP concentrations. Diamonds indicate data points of the modeled relationship between intracellular and extracellular 3-nitropropionate (3-NP) concentrations. Intracellular 3-NP concentrations ($[3\text{-NP}]_i$) were determined by adjusting their values in our model to obtain the experimentally measured cell concentrations (see Table 3) under fixed extracellular 3-NP concentrations ($[3\text{-NP}]_e$).[39] The solid line shows the linear regression for the four data points. The coefficient of determination ($R^2$) indicates how well a linear relation fits the four data points. A $F$-test[58] was used to estimate the statistical significance in the form of a $p$-value of the linear relation.

used our model framework to determine the effective intracellular 3-NP concentrations to be 0.012, 0.023, 0.063, and 0.118 mM, respectively. This was done by adjusting the intracellular 3-NP concentrations to values that reproduced the experimentally measured cell concentrations at different extracellular drug concentrations (see Table 3). The results shown in Fig. 4 suggest a linear relation ($R^2 = 0.999$) between the intracellular and extracellular 3-NP concentrations in a concentration range from 0.2 to 10.0 mM. Furthermore, we performed an $F$-test[58] analysis to examine the significance of the linear relation and obtained a $p$-value of $4.3 \times 10^{-4}$, which confirmed the statistical significance of the linearity. Because the intracellular framework contained many parameters, we performed a more robust analysis of the linearity by increasing and decreasing each parameter in *group I* (Table 2) by 50%, except for those parameters whose values cannot exceed one, and recalculating the intracellular 3-NP concentrations. Table 5 shows the calculated intracellular 3-NP concentrations, coefficients of determination ($R^2$), and the $p$-values from the $F$-test associated with changing the parameter values. With increased or decreased parameter values, the obtained intracellular 3-NP concentrations could be very different from the original ones, *e.g.*, the determined intracellular inhibitor concentrations were quite sensitive to changes in $w_{ICL1}$. However, the $R^2$ and $p$-values were always above 0.990 and below 0.050, respectively, indicating that the linear relation between the intracellular and extracellular 3-NP concentrations was robust to the changes in parameter values.

The lack of explicitly measured 3-NP concentrations in the phagosome compartments of the macrophage prevents a direct experimental verification of the linear relation proposed here. Instead, we used indirect approaches to investigate the possible mechanism that could underlie the linear relation between the intracellular and extracellular inhibitor concentrations.[27,29] When we assumed that the inhibitor molecules entered the mouse macrophages through diffusion and that, at some intracellular concentration threshold, the macrophages initiated active efflux transport of the inhibitor, we found that the steady-state intracellular and extracellular 3-NP concentrations could indeed be expressed by a linear relation (see Section S3 in the ESI† for details):

$$[3\text{-NP}]_i = K[3\text{-NP}]_e + B \quad (10)$$

where $[3\text{-NP}]_e$ denotes the extracellular 3-NP concentration, the subscript "$e$" indicates extracellular concentration, and $K$ and $B$ are constants independent of the value of $[3\text{-NP}]_e$. The linear relation between the intracellular and extracellular 3-NP concentrations is thus plausible from a cellular pharmacodynamics and pharmacokinetics standpoint. Although direct evidence for 3-NP is as yet unavailable, experimentally

 This journal is © The Royal Society of Chemistry 2011

**Table 5** Results of testing the linearity between the intracellular and extracellular 3-nitropropionate (3-NP) concentrations under variable parameter values. We characterized the linearity using coefficients of determination ($R^2$) between the intracellular and extracellular 3-nitropropionate (3-NP) concentrations. We calculated *p*-values from a *F*-test[58] analysis to examine the statistical significance of the linear relationship in the concentrations. Results for the decrease in $k_d$ were unavailable because we were unable to reproduce the experimental data in Fig. 2 for such decrease

| | | Determined $[3\text{-NP}]_i$ (mM) | | | | | |
|---|---|---|---|---|---|---|---|
| Parameter | Change | $[3\text{-NP}]_e$ = 0.2 mM | $[3\text{-NP}]_e$ = 1.0 mM | $[3\text{-NP}]_e$ = 5.0 mM | $[3\text{-NP}]_e$ = 10.0 mM | $R^2$ | *p*-value ($\times 10^{-4}$) |
| No change | | 0.012 | 0.023 | 0.063 | 0.118 | 0.999 | 4.3 |
| [SUC] | +50% | 0.016 | 0.030 | 0.078 | 0.143 | 0.999 | 4.2 |
| | −50% | 0.008 | 0.016 | 0.047 | 0.092 | 0.998 | 8.6 |
| $K_{SUC,ICL1}$ | +50% | 0.011 | 0.021 | 0.057 | 0.109 | 0.999 | 5.5 |
| | −50% | 0.016 | 0.030 | 0.079 | 0.142 | 0.999 | 4.6 |
| $K_{SUC,MCL1}$ | +50% | 0.011 | 0.021 | 0.059 | 0.112 | 0.999 | 5.0 |
| | −50% | 0.015 | 0.028 | 0.074 | 0.135 | 0.999 | 4.2 |
| $K_{SUC,ICL2}$ | +50% | 0.012 | 0.023 | 0.062 | 0.116 | 0.999 | 4.2 |
| | −50% | 0.012 | 0.023 | 0.065 | 0.124 | 0.999 | 5.5 |
| $K_{SUC,MCL2}$ | +50% | 0.012 | 0.023 | 0.063 | 0.118 | 0.999 | 4.3 |
| | −50% | 0.012 | 0.023 | 0.063 | 0.118 | 0.999 | 4.3 |
| $K_{3\text{-NP,ICL1}}$ | +50% | 0.015 | 0.029 | 0.076 | 0.138 | 0.999 | 4.3 |
| | −50% | 0.008 | 0.016 | 0.048 | 0.096 | 0.998 | 9.8 |
| $K_{3\text{-NP,MCL1}}$ | +50% | 0.014 | 0.027 | 0.072 | 0.132 | 0.999 | 4.0 |
| | −50% | 0.009 | 0.018 | 0.052 | 0.102 | 0.999 | 7.0 |
| $K_{3\text{-NP,ICL2}}$ | +50% | 0.012 | 0.024 | 0.069 | 0.139 | 0.998 | 11.5 |
| | −50% | 0.012 | 0.021 | 0.052 | 0.091 | 0.998 | 8.8 |
| $K_{3\text{-NP,MCL2}}$ | +50% | 0.012 | 0.023 | 0.063 | 0.118 | 0.999 | 4.3 |
| | −50% | 0.012 | 0.023 | 0.063 | 0.118 | 0.999 | 4.3 |
| $w_{ICL1}$ | 1 | 0.009 | 0.016 | 0.034 | 0.056 | 0.995 | 24.7 |
| | −50% | 0.026 | 0.060 | 0.179 | 0.324 | 0.999 | 6.8 |
| $w_{MCL1}$ | 1 | 0.012 | 0.023 | 0.063 | 0.118 | 0.999 | 4.4 |
| | −50% | 0.020 | 0.045 | 0.139 | 0.257 | 0.999 | 2.7 |
| $U_C$ | +50% | 0.013 | 0.025 | 0.070 | 0.124 | 0.999 | 3.7 |
| | −50% | 0.010 | 0.019 | 0.051 | 0.096 | 0.999 | 3.3 |
| $k_d$ | +50% | 0.011 | 0.020 | 0.056 | 0.106 | 0.999 | 3.9 |

measured average concentrations in macrophages exist for some inhibitors, such as β-lactams,[31,32] and the linear relationship between drug concentrations inside and outside macrophages has been experimentally verified for a β-lactam, penicillin.[31]

### Combinational effects of 3-NP and other enzyme inhibitions

The strategy of combining multiple drugs is promising from considerations of efficacy, safety, and potential reduction in emerging drug resistance.[33,59] The use of combinations of drugs could allow for a smaller dosage of each drug to achieve a given therapeutic effect or be used to boost efficacy within safe drug dose limits.[34] Although not explicitly treated here, the emergence of drug resistance through escape mutants could be reduced if different drugs affect different targets. Previous studies have shown that modeling the inhibition of metabolic pathways can help identify potential synergistic inhibitory effects of drug combinations and suggest novel drug combination therapies.[37,38]

We used the mathematical framework to computationally study the growth inhibition of *M. tuberculosis* by different combinations of two sets of "drugs" separately targeting (1) the ICL1/ICL2 and malate synthase (MS) enzymes and (2) the ICL1/ICL2 and glycerol-3-phosphate dehydrogenase (G3PD) enzymes. MS was chosen as it is considered a possible drug target for *M. tuberculosis*[17] and is part of the ICL1/ICL2 pathway. We selected G3PD because it is not part of the same pathway as ICL1/ICL2 yet is crucial for the utilization of glycerol, an intracellularly available carbon source other than fatty acids.[11,19,39] We also examined whether the *in vitro* framework used to study *M. tuberculosis* growth on propionate medium[18] was capable of exhibiting synergistic inhibition. Here, we used synergy in the sense that two or more drugs working together produce a result not obtainable by any of them independently. In the following sections, we considered the actual drug concentrations for 3-NP, but for the second inhibition we mimicked the drug action by directly reducing the flux of materials through the corresponding enzyme-catalyzed reaction.

**ICL1/ICL2-MS inhibition.** The first drug combination study analyzed the effect of 3-NP and concomitant inhibition of the MS enzyme on the growth of *M. tuberculosis*. With the assigned parameter values from Table 3, we used the mathematical framework to calculate the cell concentrations of *M. tuberculosis* after six days of growth at different 3-NP concentrations and at different degrees of inhibition of the MS enzyme. Fig. 5A shows the calculated dose-response curves when we constrained the flux through the MS enzyme to 100%, 67%, 33%, and 0% of the wild-type flux value.

In general, these curves indicated that MS inhibition was able to reduce the dose requirement of 3-NP to achieve a particular inhibitory effect. We can quantify this effect by calculating the reduction in 3-NP concentration that can achieve the same overall inhibitory effect at any given level of MS inhibition. As shown in Fig. 5A, the maximum possible effect of 3-NP alone (solid line) is a roughly two orders of magnitude reduction in cell concentration. For example, to achieve 80% of the greatest possible 3-NP inhibitory effect

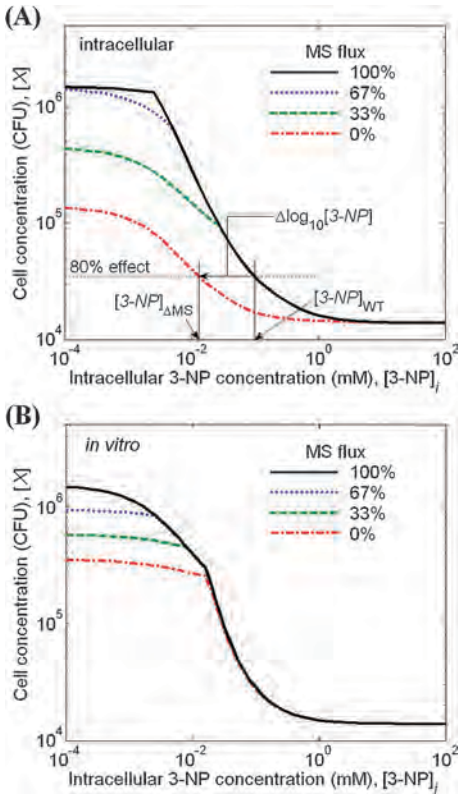


**Fig. 5** Effects of the combined inhibition of 3-nitropropionate (3-NP) and the malate synthase (MS) enzyme. *Mycobacterium tuberculosis* cell concentrations after six days of growth ([*X*]) as functions of 3-nitropropionate (3-NP) concentrations ($[3\text{-NP}]_i$) obtained from: (A) the intracellular framework and (B) the *in vitro* framework, where the flux through the malate synthase (MS) enzyme was constrained to 100%, 67%, 33%, and 0% of its wild-type flux. The "80% effect" indicates 80% of the greatest decrease in $\log_{10}[X]$ that could be achieved with 3-NP, where specifically the "greatest decrease" indicates the difference between $\log_{10}[X]$ without 3-NP and at the highest 3-NP concentration. $[3\text{-NP}]_{WT}$ represents the 3-NP concentration required to achieve the "80% 3-NP effect" without constraint on the flux through the MS enzyme, and $[3\text{-NP}]_{\Delta MS}$ represents the required 3-NP concentration with zero flux through the MS enzyme. $\Delta\log_{10}[3\text{-NP}] = \log_{10}[3\text{-NP}]_{WT} - \log_{10}[3\text{-NP}]_{\Delta MS}$. CFU, colony-forming unit.

("80% effect" in Fig. 5A) using 3-NP alone required an inhibitor concentration of $[3\text{-NP}]_{WT}$. If we constrained the flux through the MS enzyme to zero (equivalent to deleting the MS enzyme), the required 3-NP concentration to achieve the same inhibitory effect would be $[3\text{-NP}]_{\Delta MS}$. We quantitatively described this decrease in 3-NP using the following equation:

$$\Delta\log_{10}[3\text{-NP}] = \log_{10}[3\text{-NP}]_{WT} - \log_{10}[3\text{-NP}]_{\Delta MS} \quad (11)$$

Thus, with a complete inhibition of the MS enzyme, the 80% inhibition effect could be achieved by only using 13.4% ($10^{\Delta\log_{10}[3\text{-NP}]} = 10^{-0.874} = 0.134$) of the original concentration of 3-NP.

The effect of MS inhibition was not synergistic, because MS inhibition could not further reduce the pathogen cell concentration below the maximum inhibition achieved by 3-NP. This is because both the MS enzyme and 3-NP-targeted ICL1/ICL2 enzymes are all part of the glyoxylate pathway that processes isocitrate. ICL1/ICL2 converts isocitrate to glyoxylate, which, in turn, is converted by MS into *S*-malate. This pathway is required for *M. tuberculosis* to use fatty acids, the major carbon sources for the pathogen in macrophages. In essence, targeting both ICL1/ICL2 and MS enzymes inhibits the same flux through the glyoxylate pathway. Thus, one could either target ICL1/ICL2 or MS to inhibit this pathway, but no additional reduction in the growth of the pathogen would be possible using this drug combination strategy. However, it may be important to explore a different druggable target in the same pathway under certain conditions. For example, an existing drug for a particular target in the pathway might be associated with non-optimal pharmacological properties, making it desirable to either develop alternative drugs against that target or explore other druggable targets in the same pathway. Another condition could be that, if the known target enzyme were capable of mutating under drug pressure and potentially giving rise to a drug-resistant pathogen, it would be desirable to have two druggable targets in the same pathway as the likelihood of two enzyme mutations arising at the same time is considerably lower than that of any single one.

We examined how robust these observations were with respect to parameter variation in the model framework. We increased and decreased the value of each model parameter by 50% (except for those parameters whose values cannot exceed one) and calculated the resultant values for $\Delta\log_{10}[3\text{-NP}]$. Table 6 shows that the values for $\Delta\log_{10}[3\text{-NP}]$ ranged from 0.498–1.320, indicating that the required 3-NP concentration was 4.8–31.8% ($=10^{-1.320}$–$10^{-0.498}$) of $[3\text{-NP}]_{WT}$. This suggests that the observation was robust with respect to variations in the parameters of the model.

We also examined whether the previously developed *in vitro* framework[18] was associated with quantitative or qualitative differences compared with our macrophage-based model. Fig. 5B shows the calculated dose-response curves and indicates that the inhibition of the MS enzyme did not influence the dose-response curves as much as in Fig. 5A. This decreased effect stems from the ICL reaction not playing a crucial role under the *in vitro* condition. In the simulated *in vitro* conditions, propionate, a fatty acid, is the main carbon source,[18] and the utilization of propionate mainly depends on the MCL reaction[18] and not on the ICL reaction.

**ICL1/ICL2-G3PD inhibition.** The second drug combination used 3-NP as the primary drug and modeled the inhibition of the G3PD enzyme as the second target. We used the same mathematical framework and parameters used in the ICL1/ICL2-MS study above to calculate the cell concentrations of *M. tuberculosis* after six days of growth at different 3-NP concentrations and at different degrees of inhibition of the G3PD enzyme. Fig. 6A shows the calculated dose-response curves when we constrained the flux through the G3PD enzyme to 100%, 67%, 33%, and 0% of the wild-type flux values.

One can note two key features from this curve: (1) fully inhibiting the G3PD enzyme by itself at insignificant 3-NP concentrations did not significantly reduce *M. tuberculosis* growth; and (2) at higher 3-NP concentrations, inhibition of G3PD further reduces growth beyond what was possible with


This journal is © The Royal Society of Chemistry 2011

**Table 6** Effects of the parameter values on the drug combinations. $\Delta\log_{10}$[3-NP] indicates the difference between $\log_{10}[\text{3-NP}]_{WT}$ and $\log_{10}[\text{3-NP}]_{\Delta MS}$, where $[\text{3-NP}]_{WT}$ represents the 3-nitropropionate (3-NP) concentration required to obtain an 80% inhibitory effect of 3-NP without the inhibition of the malate synthase (MS) enzyme and $[\text{3-NP}]_{\Delta MS}$ represents the required 3-NP concentration with full inhibition of the enzyme. $\Delta\log_{10}[X]$ indicates the difference between $\log_{10}[X]_{WT}$ and $\log_{10}[X]_{\Delta G3PD}$, where $[X]_{WT}$ represents the cell concentrations of *M. tuberculosis* at a high 3-NP concentration ($10^2$ mM) in the absence of inhibition of the glycerol-3-phosphate dehydrogenase (G3PD) enzyme and $[X]_{\Delta G3PD}$ represents the cell concentration under full inhibition of the G3PD enzyme

| | | Inhibition of MS | | Inhibition of G3PD | |
|---|---|---|---|---|---|
| Parameter | Change | $\Delta\log_{10}$[3-NP] | $[\text{3-NP}]_{\Delta MS}/[\text{3-NP}]_{WT}$(%) | $\Delta\log_{10}[X]$ | $[X]_{\Delta G3PD}/[X]_{WT}$(%) |
| Original values | | 0.874 | 13.4 | 0.417 | 38.3 |
| [SUC] | +50% | 0.844 | 14.3 | 0.417 | 38.3 |
| | −50% | 0.922 | 12.0 | 0.417 | 38.3 |
| $K_{SUC,ICL1}$ | +50% | 0.839 | 14.5 | 0.417 | 38.3 |
| | −50% | 0.961 | 10.9 | 0.417 | 38.3 |
| $K_{SUC,MCL1}$ | +50% | 0.951 | 11.2 | 0.417 | 38.3 |
| | −50% | 0.728 | 18.7 | 0.417 | 38.3 |
| $K_{SUC,ICL2}$ | +50% | 0.867 | 13.6 | 0.417 | 38.3 |
| | −50% | 0.895 | 12.7 | 0.417 | 38.3 |
| $K_{SUC,MCL2}$ | +50% | 0.874 | 13.4 | 0.417 | 38.3 |
| | −50% | 0.874 | 13.4 | 0.417 | 38.3 |
| $K_{3\text{-NP,ICL1}}$ | +50% | 0.947 | 11.3 | 0.417 | 38.3 |
| | −50% | 0.776 | 16.7 | 0.417 | 38.3 |
| $K_{3\text{-NP,MCL1}}$ | +50% | 0.751 | 17.7 | 0.417 | 38.3 |
| | −50% | 1.109 | 7.8 | 0.417 | 38.3 |
| $K_{3\text{-NP,ICL2}}$ | +50% | 0.939 | 11.5 | 0.417 | 38.3 |
| | −50% | 0.773 | 16.9 | 0.417 | 38.3 |
| $K_{3\text{-NP,MCL2}}$ | +50% | 0.874 | 13.4 | 0.417 | 38.3 |
| | −50% | 0.874 | 13.4 | 0.417 | 38.3 |
| $w_{ICL1}$ | 1 | 0.566 | 27.2 | 0.417 | 38.3 |
| | −50% | 1.320 | 4.8 | 0.417 | 38.3 |
| $w_{MCL1}$ | 1 | 0.874 | 13.4 | 0.417 | 38.3 |
| | −50% | 0.498 | 31.8 | 0.417 | 38.3 |
| $U_{Fat}$ | +50% | 0.927 | 11.8 | 0.390 | 40.7 |
| | −50% | 0.708 | 19.6 | 0.443 | 36.1 |
| $U_{Glyc}$ | +50% | 0.822 | 15.1 | 0.653 | 22.3 |
| | −50% | 0.922 | 12.0 | 0.180 | 66.0 |
| $U_C$ | +50% | 0.851 | 14.1 | 0.415 | 38.4 |
| | −50% | 0.906 | 12.4 | 0.405 | 39.4 |
| $\log_{10}[X](t_0)$ | +50% | 0.874 | 13.4 | 0.417 | 38.3 |
| | −50% | 0.874 | 13.4 | 0.417 | 38.3 |
| $k_d$ | +50% | 0.874 | 13.4 | 0.417 | 38.3 |
| | −50% | 0.874 | 13.4 | 0.417 | 38.3 |
| $\tau$ | +50% | 0.874 | 13.4 | 0.382 | 41.5 |
| | −50% | 0.874 | 13.4 | 0.451 | 35.4 |

3-NP alone. Thus, we have the situation where inhibition of a non-essential enzyme potentiates the action of 3-NP in a synergistic manner.

We quantified this effect at a 3-NP concentration of $10^2$ mM by calculating the additional reduction in cell concentration $\Delta\log_{10}[X]$ when the G3PD flux was constrained to zero:

$$\Delta\log_{10}[X] = \log_{10}[X]_{WT} - \log_{10}[X]_{\Delta G3PD} \qquad (12)$$

where $[X]_{WT}$ denotes the calculated cell concentrations in the presence of $[\text{3-NP}]_i = 10^2$ mM and $[X]_{\Delta G3PD}$ denotes cell concentrations in the presence of both "drugs." The additional reduction in cell growth beyond what was achievable with 3-NP alone was 38.3% ($10^{\Delta\log_{10}[X]} = 10^{-0.417} = 0.383$). The synergistic effect stems from the utilization of both fatty acids (targeted by 3-NP) and glycerol (affected by G3PD inhibition) as carbon sources for *M. tuberculosis* in macrophages.[11,19,39] The pathways processing these carbon sources are not directly connected, and the fluxes through these enzyme reactions are much more independent than what was the case for ICL1/ICL2-MS enzymes in the glyoxylate shunt.

Similar to the ICL1/ICL2-MS inhibition, we examined whether the parameter values in the intracellular framework affected the observed synergistic effect in the ICL1/ICL2-G3PD inhibition combination. Table 6 shows that the changes of most parameters did not affect the values of $\Delta\log_{10}[X]$. Only the variation in the upper limit of glycerol uptake ($U_{Glyc}$) significantly changed the value of $\Delta\log_{10}[X]$, suggesting that the synergistic effect of 3-NP and G3PD inhibition mainly depended on the uptake of glycerol. Conversely, the observed effect on *M. tuberculosis* would only be present when glycerol is an important nutrient source in the macrophage.

We also compared the modeled effects with the previously developed *in vitro* framework.[18] Fig. 6B shows that the calculated dose-response curves did not show any synergistic effects in that the additional inhibition of the G3PD flux could not decrease the growth of *M. tuberculosis* beyond 3-NP inhibition. The reason for this behavior is that the *in vitro* medium contains different nutrient sources. Thus, when constraining the G3PD flux to 33% of its wild-type value, the cell concentration [*X*] was independent of 3-NP concentrations

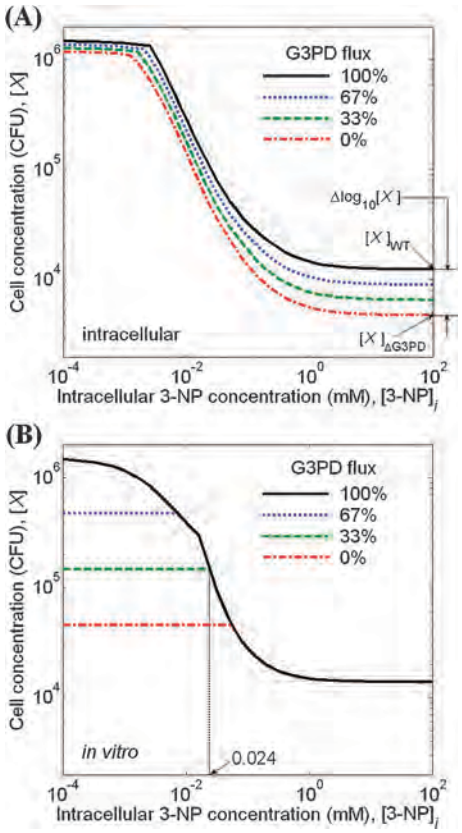


**Fig. 6** Effects of the combined inhibition of 3-nitropropionate (3-NP) and the glycerol-3-phosphate dehydrogenase (G3PD) enzyme. *Mycobacterium tuberculosis* cell concentrations after six days of growth ([*X*]) as functions of 3-NP concentrations ([3-NP]$_i$) obtained from: (A) the intracellular framework and (B) the *in vitro* framework, where the flux through the glycerol-3-phosphate dehydrogenase (G3PD) enzyme was constrained to 100%, 67%, 33%, and 0% of its wild-type flux. $[X]_{WT}$ represents the cell concentration at $10^2$ mM 3-NP, when there was no constraint on the flux through the G3PD enzyme, and $[X]_{\Delta G3PD}$ represents the cell concentration when the flux through the G3PD enzyme was constrained to zero. $\Delta\log_{10}[X] = \log_{10}[X]_{WT} - \log_{10}[X]_{\Delta G3PD}$. CFU, colony-forming unit.

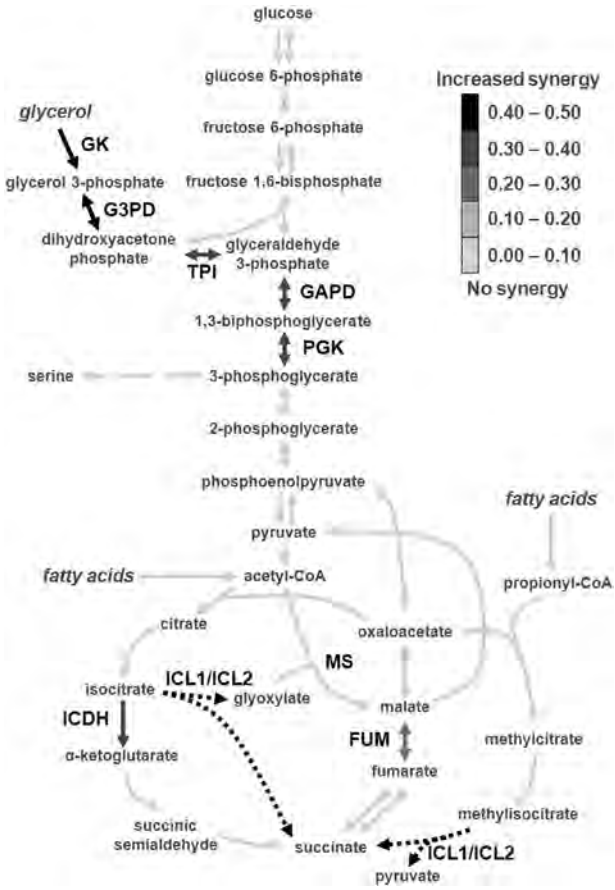


**Fig. 7** Calculated level of synergy between 3-NP and each reaction in the central carbon metabolism of *Mycobacterium tuberculosis*. The dotted arrows indicate reactions that are catalyzed by the isocitrate lyase 1 (ICL1) and isocitrate lyase 2 (ICL2) enzymes and thus targeted by 3-nitropropionate (3-NP). Solid arrows represent other reactions in the central carbon metabolism, and the color intensity indicates the synergy levels of the corresponding reactions with 3-NP. For each reaction RXN, the synergy level was computed using the value for $\Delta\log_{10}[X] = \min(\log_{10}[X]_{WT}, \log_{10}[X]_{0,\Delta RXN}) - \log_{10}[X]_{\Delta RXN}$, where $[X]_{WT}$ represents the cell concentration at $10^2$ mM 3-NP, $[X]_{0,\Delta RXN}$ represents the cell concentration at the zero 3-NP concentration level with the flux through the reaction RXN constrained to zero, and $[X]_{\Delta RXN}$ represents the cell concentration at $10^2$ mM 3-NP with the flux through the reaction RXN constrained to zero. FUM, fumarase; G3PD, glycerol-3-phosphate dehydrogenase; GAPD, glyceraldehydes-3-phosphate dehydrogenase; GK, glycerol kinase; ICDH, isocitrate dehydrogenase; MS, malate synthase; PGK, phosphoglycerate kinase; TPI, triose phosphate isomerase.

lower than 0.024 mM, indicating that the primary inhibition mechanisms under these conditions were through the G3PD catalyzed reaction. At a 3-NP concentration higher than 0.024 mM, the dose-response curve indicates that the inhibition was independent of the G3PD reaction and solely driven by 3-NP inhibition. In the *in vitro* propionate medium, *M. tuberculosis* synthesizes glycerol-3-phosphate from propionate through a serial set of reactions, including the MCL reaction (inhibited by 3-NP) and the G3PD-catalyzed reaction. When we placed constraints on the fluxes of a set of serially connected reactions, only the strictest constraint affected the calculated cell concentrations of *M. tuberculosis*, and, hence, no synergistic effects were possible.

### Overall assessment of ICL1/ICL2 inhibition partners

To examine other possible non-intuitive synergistic inhibition partners with ICL1/ICL2 among the metabolic enzymes and pathways in *M. tuberculosis*, we calculated $\Delta\log_{10}[X]$ for the inhibition of each reaction in the *iNJ*661i metabolic network (provided in the ESI† as Delta_log10X_all_011311.xls). The top seven reactions with the largest $\Delta\log_{10}[X]$ values were all associated with the central carbon metabolism pathways, highlighting the importance of these pathways in providing possible synergistic targets. Fig. 7 shows the predicted synergistic level of each reaction in combination with 3-NP in the central carbon metabolism of *M. tuberculosis*. Two reactions in the glycerol-processing pathway, catalyzed by glycerol kinase (GK) and G3PD, respectively, ranked as the top two reactions in terms of $\Delta\log_{10}[X]$, indicating the key role of this pathway in inducing synergistic effects under *in vivo* conditions with the 3-NP glyoxylate shunt inhibitor. The obtained dose-response


This journal is © The Royal Society of Chemistry 2011

curves for jointly inhibiting ICL1/ICL2-GK were similar to those in the ICL1/ICL2-G3PD study (results not shown), suggesting that the entire glycerol-processing pathway and possible regulatory mechanisms of this pathway could be considered synergistic drug-targets with 3-NP. The reactions, catalyzed by triose phosphate isomerase (TPI), glyceraldehyde 3-phosphate dehydrogenase (GAPD), and phosphoglycerate kinase (PGK), had moderately high synergistic levels. These reactions were necessary for the synthesis of serine precursors from glycerol when we blocked the synthesis routes from fatty acids by 3-NP inhibition. The last two reactions associated with synergistic inhibition in the central carbon metabolism were catalyzed by isocitrate dehydrogenase (ICDH) and fumarase (FUM) as part of the tricarboxylic acid (TCA) cycle. While inhibiting the MS enzyme in the glyoxylate shunt pathway did not provide synergistic benefits, inhibition of these additional targets blocked the TCA cycle through which the bacterium utilizes fatty acids as carbon sources. Thus, inhibition of the glyoxylate shunt in the macrophage environment highlighted the importance of *M. tuberculosis* pathways converting glycerol to other metabolites and selected parts of the TCA cycle for the growth and viability of the pathogen. It is necessary, however, to verify our predictions of synergy and validate their importance in different experimental settings before proceeding with a targeted drug-development effort against pairs or combinations of metabolic pathway targets.

## Conclusion

The major promise of a systems biology approach lies in the ability to determine and describe emergent properties of a system from an underlying description of each of its components. Attractive as a concept and highly relevant to complex problems, such as cancer, traumatic brain injury, and infectious diseases, systems biology can provide the framework to understand the relationships among a multitude of cellular components. Translating these concepts into quantitative and qualitative computational models impacts both rational target selection and understanding systemic effects of drugs. Our work, focusing on the metabolic adjustments required of intracellular pathogens when colonizing within *in vitro, ex vivo*, and *in vivo* environments, presents a novel construct to realize both quantitative models and qualitative insights based on a systems-level description of metabolism.

The adjustment of an organism's lifestyle and metabolism to different environmental queues is a necessary survival strategy evoked by all intracellular pathogens. Similarly, the response of a pathogen to small molecule inhibitors will also non-trivially depend on the environment, *e.g.*, inhibiting an enzyme that is no longer required because of an altered uptake of carbon sources will have no effect on the survival or growth of the organism. Our ability to quantitatively model this behavior *via* dose-response curves for *M. tuberculosis* paves the way to prospectively characterize potential drug targets and their relevance in different host environments.

A potential barrier to systems biology studies is the presence of many different parameters that are not directly available from experimental studies but need to be estimated from model studies. One needs to strike a balance between the quantitative and qualitative aspects of systems biology modeling with the availability of experimental data and parameters. Here, we mitigated this problem by performing extensive parameter sensitivity analyses to verify that our results and insights were robust to changes in the parameter values. We feel that the promise of systems biology will be fulfilled by both being able to use complex models to create very specific quantitative predictions as well as in creating qualitative predictions that yield specific well-defined testable hypotheses. This is the balance we have tried to strike in the current work: specific quantitative model of the inhibitory effect of 3-NP on *M. tuberculosis* growth inside murine macrophages and a more qualitative discussion on possible synergistic targets based on metabolic considerations, *e.g.*, the relative importance of the glycerol-processing pathway under limiting nutritional conditions and when targeting the glyoxylate shunt with drugs.

Ultimately, the ability to model the dynamics of host-pathogen interactions under *in vivo* conditions by incorporating more extensive metabolic, signaling, and transcriptional regulatory network models will provide a platform for both host and pathogen drug-target identification that optimally selects potent and safe drug combinations.

## Acknowledgements

We thank Dr F. Vital-Lopez for a careful reading of the manuscript. This project was funded in part by a competitive In-house Laboratory Independent Research (ILIR) award by the U.S. Army Assistant Secretary of the Army for Acquisition, Logistics, and Technology (ASAALT). The opinions and assertions contained herein are the private views of the authors and are not to be construed as official or as reflecting the views of the U.S. Army or the U.S. Department of Defense. This paper has been approved for public release with unlimited distribution.

## References

1 S. H. Gillespie, *Biochem. Soc. Trans.*, 2007, **35**, 1317–1320.
2 WHO, Global tuberculosis control: a short update to the 2009 report, 2009.
3 J. van den Boogaard, G. S. Kibiki, E. R. Kisanga, M. J. Boeree and R. E. Aarnoutse, *Antimicrob. Agents Chemother.*, 2009, **53**, 849–862.
4 D. B. Young, M. D. Perkins, K. Duncan and C. E. Barry 3rd, *J. Clin. Invest.*, 2008, **118**, 1255–1265.
5 A. M. Ginsberg and M. Spigelman, *Nat. Med.*, 2007, **13**, 290–294.
6 A. M. Feist, M. J. Herrgard, I. Thiele, J. L. Reed and B. O. Palsson, *Nat. Rev. Microbiol.*, 2009, **7**, 129–143.
7 R. Breitling, D. Vitkup and M. P. Barrett, *Nat. Rev. Microbiol.*, 2008, **6**, 156–161.
8 I. Thiele, T. D. Vo, N. D. Price and B. O. Palsson, *J. Bacteriol.*, 2005, **187**, 5818–5830.
9 A. Navid and E. Almaas, *Mol. BioSyst.*, 2009, **5**, 368–375.
10 A. Raghunathan, J. Reed, S. Shin, B. Palsson and S. Daefler, *BMC Syst. Biol.*, 2009, **3**, 38.
11 N. Jamshidi and B. O. Palsson, *BMC Syst. Biol.*, 2007, **1**, 26.
12 D. J. Beste, T. Hooper, G. Stewart, B. Bonde, C. Avignone-Rossa, M. E. Bushell, P. Wheeler, S. Klamt, A. M. Kierzek and J. McFadden, *Genome Biol.*, 2007, **8**, R89.
13 A. M. Feist, C. S. Henry, J. L. Reed, M. Krummenacker, A. R. Joyce, P. D. Karp, L. J. Broadbelt, V. Hatzimanikatis and B. O. Palsson, *Mol. Syst. Biol.*, 2007, **3**, 121.

14 N. C. Duarte, M. J. Herrgard and B. O. Palsson, *Genome Res*., 2004, **14**, 1298–1309.
15 I. Famili, J. Forster, J. Nielsen and B. O. Palsson, *Proc. Natl. Acad. Sci. U. S. A*., 2003, **100**, 13134–13139.
16 A. K. Chavali, J. D. Whittemore, J. A. Eddy, K. T. Williams and J. A. Papin, *Mol. Syst. Biol*., 2008, **4**, 177.
17 K. Mdluli and M. Spigelman, *Curr. Opin. Pharmacol*., 2006, **6**, 459–467.
18 X. Fang, A. Wallqvist and J. Reifman, *BMC Syst. Biol*., 2009, **3**, 92.
19 E. J. Munoz-Elias and J. D. McKinney, *Cell Microbiol*., 2006, **8**, 10–22.
20 B. B. Finlay and S. Falkow, *Microbiol. Mol. Biol. Rev*., 1997, **61**, 136–169.
21 D. Schnappinger, S. Ehrt, M. I. Voskuil, Y. Liu, J. A. Mangan, I. M. Monahan, G. Dolganov, B. Efron, P. D. Butcher, C. Nathan and G. K. Schoolnik, *J. Exp. Med*., 2003, **198**, 693–704.
22 J. J. De Voss, K. Rutter, B. G. Schroeder, H. Su, Y. Zhu and C. E. Barry, 3rd, *Proc. Natl. Acad. Sci. U. S. A*., 2000, **97**, 1252–1257.
23 P. M. Tulkens, *Eur. J. Clin. Microbiol. Infect. Dis*., 1991, **10**, 100–106.
24 G. L. Mandell, *Pharmacotherapy*, 2005, **25**, 130S–133S.
25 K. Sato, H. Tomioka, C. Sano, T. Shimizu, K. Sano, K. Ogasawara, S. Cai and T. Kamei, *J. Antimicrob. Chemother*., 2003, **52**, 199–203.
26 D. Ordway, M. Viveiros, C. Leandro, R. Bettencourt, J. Almeida, M. Martins, J. E. Kristiansen, J. Molnar and L. Amaral, *Antimicrob. Agents Chemother*., 2003, **47**, 917–922.
27 F. Van Bambeke, M. Barcia-Macay, S. Lemaire and P. M. Tulkens, *Curr. Opin. Drug Discovery Dev*., 2006, **9**, 218–230.
28 S. Carryn, H. Chanteux, C. Seral, M. P. Mingeot-Leclercq, F. Van Bambeke and P. M. Tulkens, *Infect. Dis. Clin. North Am*., 2003, **17**, 615–634.
29 F. Van Bambeke, J. M. Michot and P. M. Tulkens, *J. Antimicrob. Chemother*., 2003, **51**, 1067–1077.
30 J. M. Michot, F. Van Bambeke, M. P. Mingeot-Leclercq and P. M. Tulkens, *Antimicrob. Agents Chemother*., 2004, **48**, 2673–2682.
31 D. B. Lowrie, V. R. Aber and M. E. Carrol, *J. Gen. Microbiol*., 1979, **110**, 409–419.
32 S. Carryn, F. Van Bambeke, M. P. Mingeot-Leclercq and P. M. Tulkens, *Antimicrob. Agents Chemother*., 2002, **46**, 2095–2103.
33 M. C. Berenbaum, *Pharmacol. Rev*., 1989, **41**, 93–141.
34 G. R. Zimmermann, J. Lehar and C. T. Keith, *Drug. Discovery Today*, 2007, **12**, 34–42.
35 P. Chen, J. Gearhart, M. Protopopova, L. Einck and C. A. Nacy, *J. Antimicrob. Chemother*., 2006, **58**, 332–337.
36 P. Csermely, V. Agoston and S. Pongor, *Trends Pharmacol. Sci*., 2005, **26**, 178–182.
37 J. Lehar, G. R. Zimmermann, A. S. Krueger, R. A. Molnar, J. T. Ledell, A. M. Heilbut, G. F. Short, 3rd, L. C. Giusti, G. P. Nolan, O. A. Magid, M. S. Lee, A. A. Borisy, B. R. Stockwell and C. T. Keith, *Mol. Syst. Biol*., 2007, **3**, 80.
38 J. Lehar, A. S. Krueger, W. Avery, A. M. Heilbut, L. M. Johansen, E. R. Price, R. J. Rickles, G. F. Short, 3rd, J. E. Staunton, X. Jin, M. S. Lee, G. R. Zimmermann and A. A. Borisy, *Nat. Biotechnol*., 2009, **27**, 659–666.
39 E. J. Munoz-Elias and J. D. McKinney, *Nat. Med*., 2005, **11**, 638–644.
40 F. H. Armstrong and K. C. Fisher, *J. Gen. Physiol*., 1947, **30**, 279–289.
41 E. J. Munoz-Elias, A. M. Upton, J. Cherian and J. D. McKinney, *Mol. Microbiol*., 2006, **60**, 1109–1122.
42 T. A. Gould, H. van de Langemheen, E. J. Munoz-Elias, J. D. McKinney and J. C. Sacchettini, *Mol. Microbiol*., 2006, **61**, 940–947.
43 J. L. Hjersted, M. A. Henson and R. Mahadevan, *Biotechnol. Bioeng*., 2007, **97**, 1190–1204.
44 X. Fang, A. Wallqvist and J. Reifman, *BMC Syst. Biol*., 2010, **4**, 160.
45 M. Durot, F. Le Fevre, V. de Berardinis, A. Kreimeyer, D. Vallenet, C. Combe, S. Smidtas, M. Salanoubat, J. Weissenbach and V. Schachter, *BMC Syst. Biol*., 2008, **2**, 85.
46 A. R. Zomorrodi and C. D. Maranas, *BMC Syst. Biol*., 2010, **4**, 178.
47 J. Rengarajan, B. R. Bloom and E. J. Rubin, *Proc. Natl. Acad. Sci. U. S. A*., 2005, **102**, 8327–8332.
48 S. A. Becker, A. M. Feist, M. L. Mo, G. Hannum, B. O. Palsson and M. J. Herrgard, *Nat. Protocols*, 2007, **2**, 727–738.
49 J. S. Edwards and B. O. Palsson, *Biotechnol. Bioeng*., 1998, **58**, 162–169.
50 K. Raman and N. Chandra, *Briefings Bioinf*., 2009, **10**, 435–449.
51 E. Grafahrend-Belau, F. Schreiber, D. Koschutzki and B. H. Junker, *Plant Physiol*., 2009, **149**, 585–598.
52 D. J. Austin, N. J. White and R. M. Anderson, *J. Theor. Biol*., 1998, **194**, 313–339.
53 J. F. Moffat and L. S. Tompkins, *Infect. Immun*., 1992, **60**, 296–301.
54 S. Sahle, P. Mendes, S. Hoops and U. Kummer, *Philos. Trans. R. Soc., A*, 2008, **366**, 3619–3631.
55 N. A. van Riel, *Briefings Bioinf*., 2006, **7**, 364–374.
56 A. Bordbar, N. E. Lewis, J. Schellenberger, B. O. Palsson and N. Jamshidi, *Mol. Syst. Biol*., 2010, **6**, 422.
57 L. P. de Carvalho, S. M. Fischer, J. Marrero, C. Nathan, S. Ehrt and K. Y. Rhee, *Chem. Biol*., 2010, **17**, 1122–1131.
58 G. R. Norman and D. L. Streiner, *PDQ Statistics*, BC Decker, Inc., Hamilton, Cananda, 3rd edn., 2003.
59 J. H. Gaddum, *Pharmacology*, Oxford University Press, London, 1940.

 This journal is © The Royal Society of Chemistry 2011